Supplementary Information

Cancer-specific innate and adaptive immune rewiring drives resistance to PD-1 blockade in classic Hodgkin lymphoma

Julia Paczkowska[1*], Ming Tang[2,7*], Kyle T. Wright[3,8*], Li Song[2,9], Kelsey Luu[2,10], Vignesh Shanmugam[3,4], Emma L. Welsh[3,5], Jason L. Weirather[2], Naomi Besson[3,5], Harrison Olszewski[3,5], Billie A. Porter[3,5], Kathleen L. Pfaff[3,5], Robert A. Redd[2], Fathima Zumla Cader[1,11], Elisa Mandato[1], Jing Ouyang[1,12], Eleonora Calabretta[1], Gali Bai[2,13], Lee N. Lawton[1], Philippe Armand[1], Scott J. Rodig[3,5], Xiaole Shirley Liu[2,6,14] and Margaret A. Shipp[1#]

[1]Department of Medical Oncology, Dana-Farber Cancer Institute, Boston, MA, USA;
[2]Department of Data Science, Dana-Farber Cancer Institute, Boston, MA, USA;
[3]Department of Pathology, Brigham and Women's Hospital, Boston, MA, USA;
[4]Cancer Program, Broad Institute of MIT and Harvard, Cambridge, MA, USA;
[5]Center for Immuno-Oncology, Dana-Farber Cancer Institute, Boston, MA, USA;
[6]Harvard T.H. Chan School of Public Health, Boston, MA, USA
[7]Present address: Immunitas Therapeutics, Waltham, MA, USA;
[8]Present address: Department of Pathology, University of Oklahoma Health Sciences Center, Oklahoma City, OK, USA;
[9]Present address: Department of Biomedical Data Science, Dartmouth College, Hanover, NH, USA
[10]Present address: PathAI, Boston, MA, USA
[11]Present address: AstraZeneca, City House, Cambridge, UK
[12]Present address: Mechanisms of Cancer Resistance Thematic Center, Bristol Myers Squibb, Cambridge, MA, USA
[13]Present address: Department of Biomolecular Engineering, University of California, Santa Cruz, Santa Cruz, CA, USA
[14]Present address: GV20 Therapeutics, LLC, Cambridge, MA, USA

[*]These authors contributed equally
[#]Corresponding author: Margaret_Shipp@dfci.harvard.edu

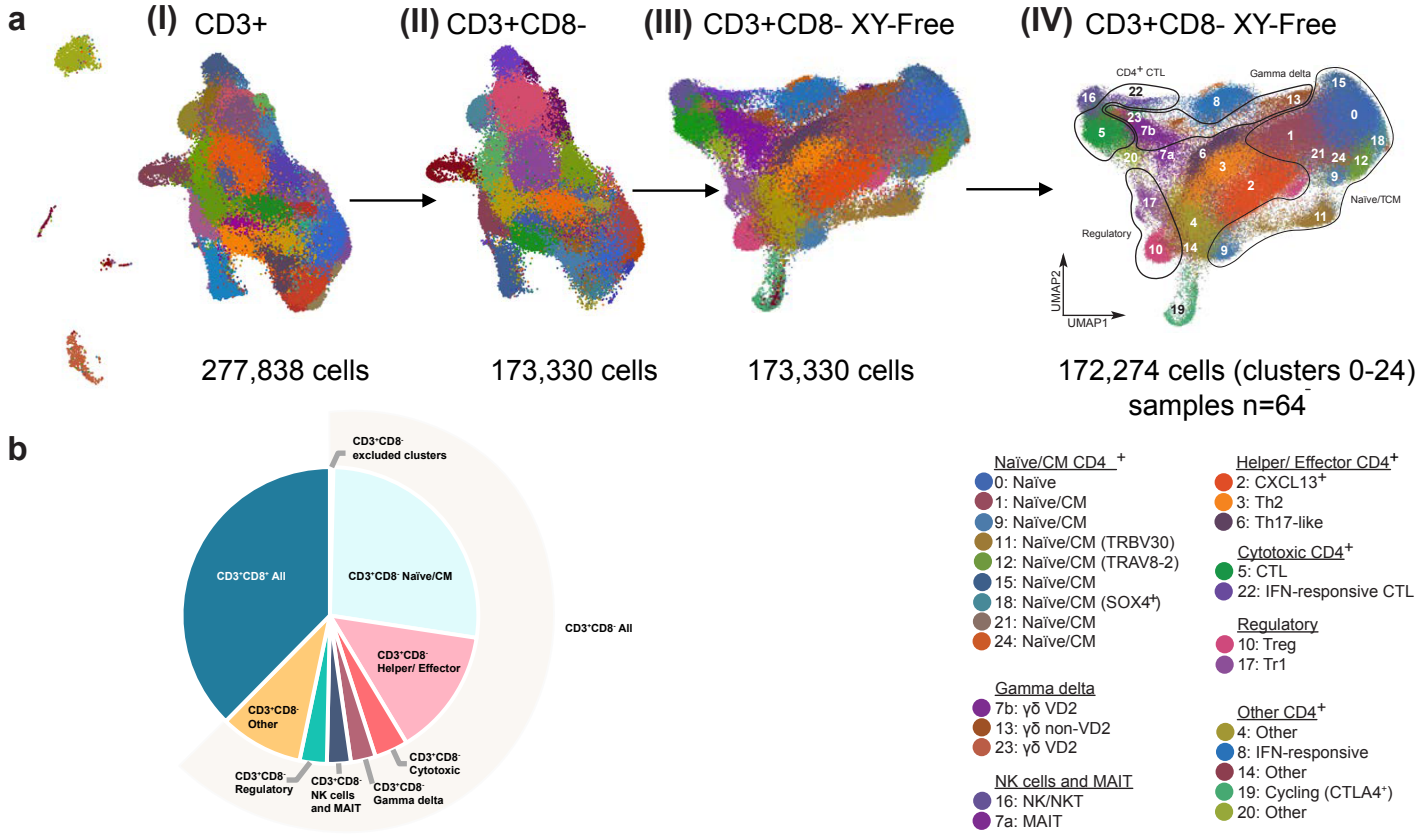

Supplementary Figure 1. Identification of circulating CD3⁺CD8⁻ (CD4⁺-enriched) immune cell populations. a Strategy to obtain the CD3⁺CD8⁻ (CD4⁺-enriched) space. (I) Uniform Manifold Approximation and Projection (UMAP) of CD3⁺ single-cell expression profiles (n=277,838 individual cells); (II) Computational removal of all *CD8A*- or *CD8B*-expressing cells (n=173,330 cells); (III) Reclustering of newly obtained CD3⁺CD8⁻ (CD4⁺-enriched) cells, visualized on UMAP; (IV) Exclusion of clusters that did not meet the inclusion criteria (see Methods) and annotation of the remained clusters (n=172,274 cells, clusters 0-24). **b** Composition of all CD3⁺ cells. **c** UMAP of CD3⁺CD8⁻ (CD4⁺-enriched) single-cell expression profiles (n=172,274 individual cells) split by groups with the indicated number of cells and samples: HD, patients with ND cHL, R/R CR at C1D1, R/R CR at C4D1, R/R PR at C1D1, R/R PR at C4D1, R/R PD at C1D1, R/R PD at C4D1. Source data are provided as a Source Data file.

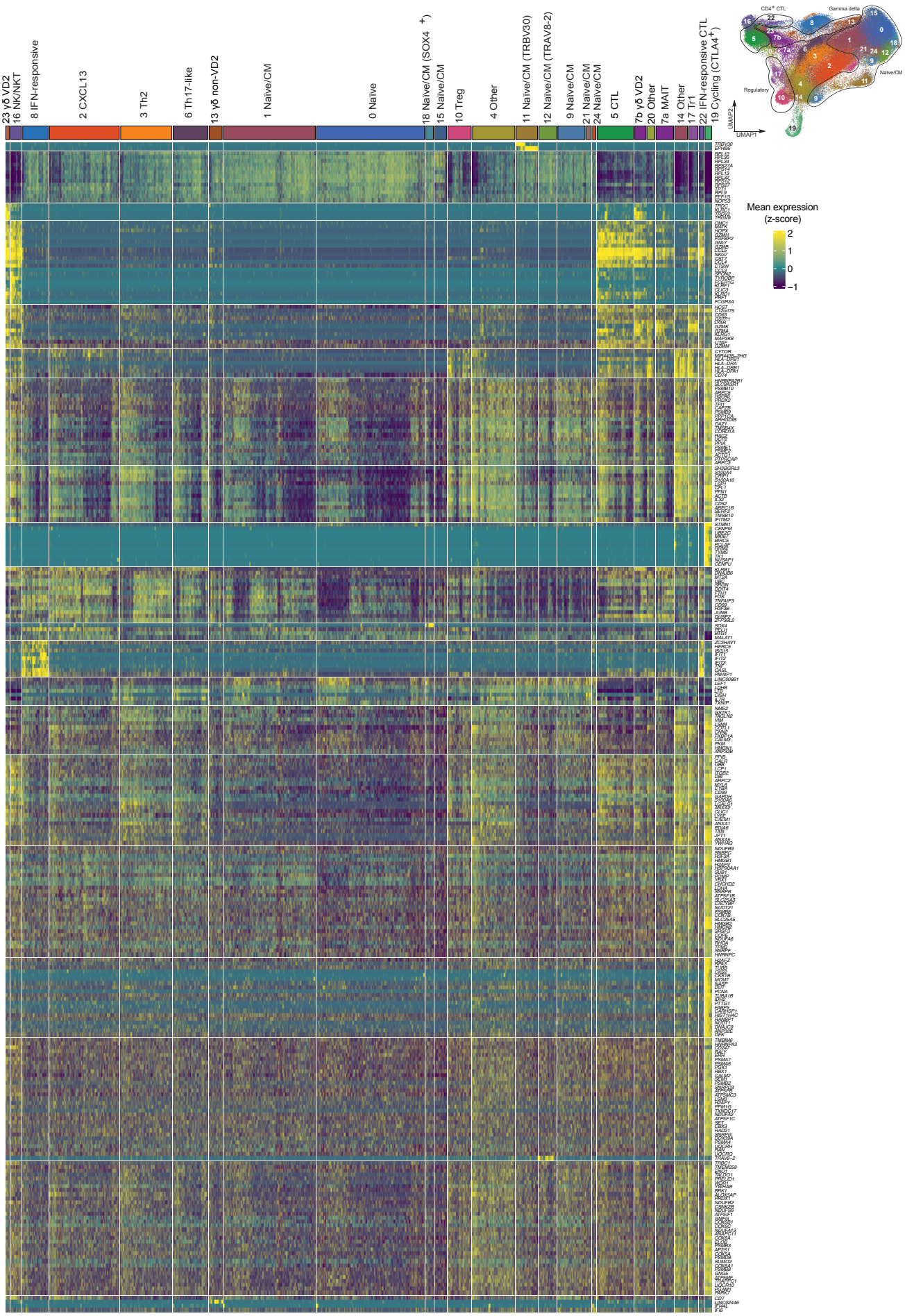

Supplementary Figure 2. Differential expression of marker genes in circulating CD3⁺CD8⁻ (CD4⁺-enriched) immune cell clusters. Heatmap showing the relative expression (z-score normalized per gene) of the top differentially expressed genes that defined clusters in CD3⁺CD8⁻ space (a two-sided Wilcoxon rank sum test, adjusted for multiple comparisons, adj p <0.05, fold change >1.75).

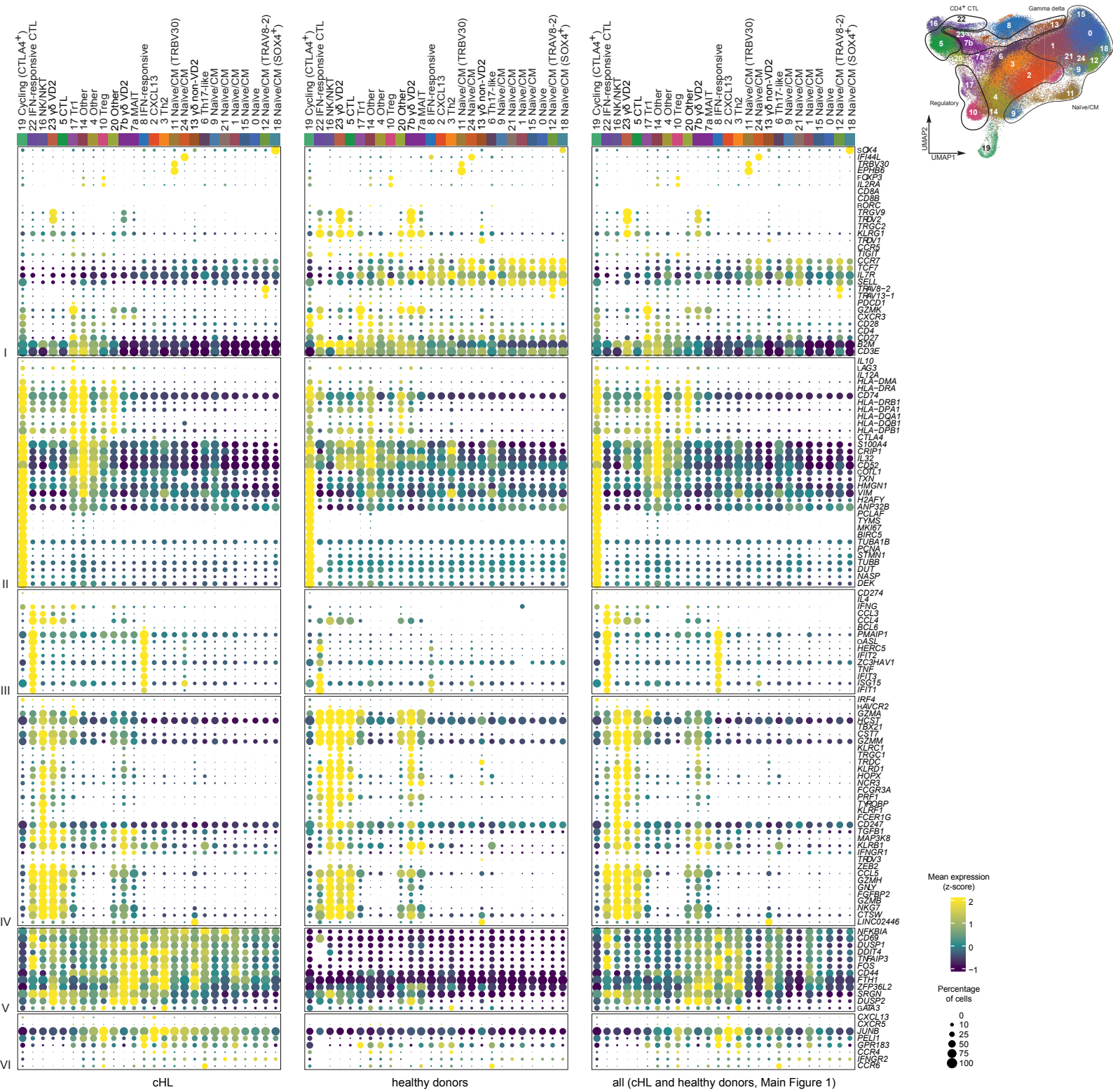

Supplementary Figure 3. Relative expression of marker genes in circulating CD3⁺CD8⁻ (CD4⁺-enriched) immune cell clusters in healthy donors, patients with cHL (newly diagnosed and relapsed/refractory) and the full cohort. Dot plot with relative expression of selected genes in CD3⁺CD8⁻ clusters split by groups: all patients with cHL (newly diagnosed and relapsed/ refractory) (left, n=51 samples), healthy donors (middle, n= 13 samples) and all patients with cHL and healthy donors together (right, n=64 samples). Displayed genes were curated from the top differentially expressed genes that defined clusters using a two-sided Wilcoxon rank sum test, adjusted for multiple comparisons (adj p <0.05, fold change >1.75) and supplemented with relevant markers based on *a priori* knowledge. The size of the dot indicates the percentage of marker-expressing cells in each cluster and the z-score reflects mean marker expression across the clusters.

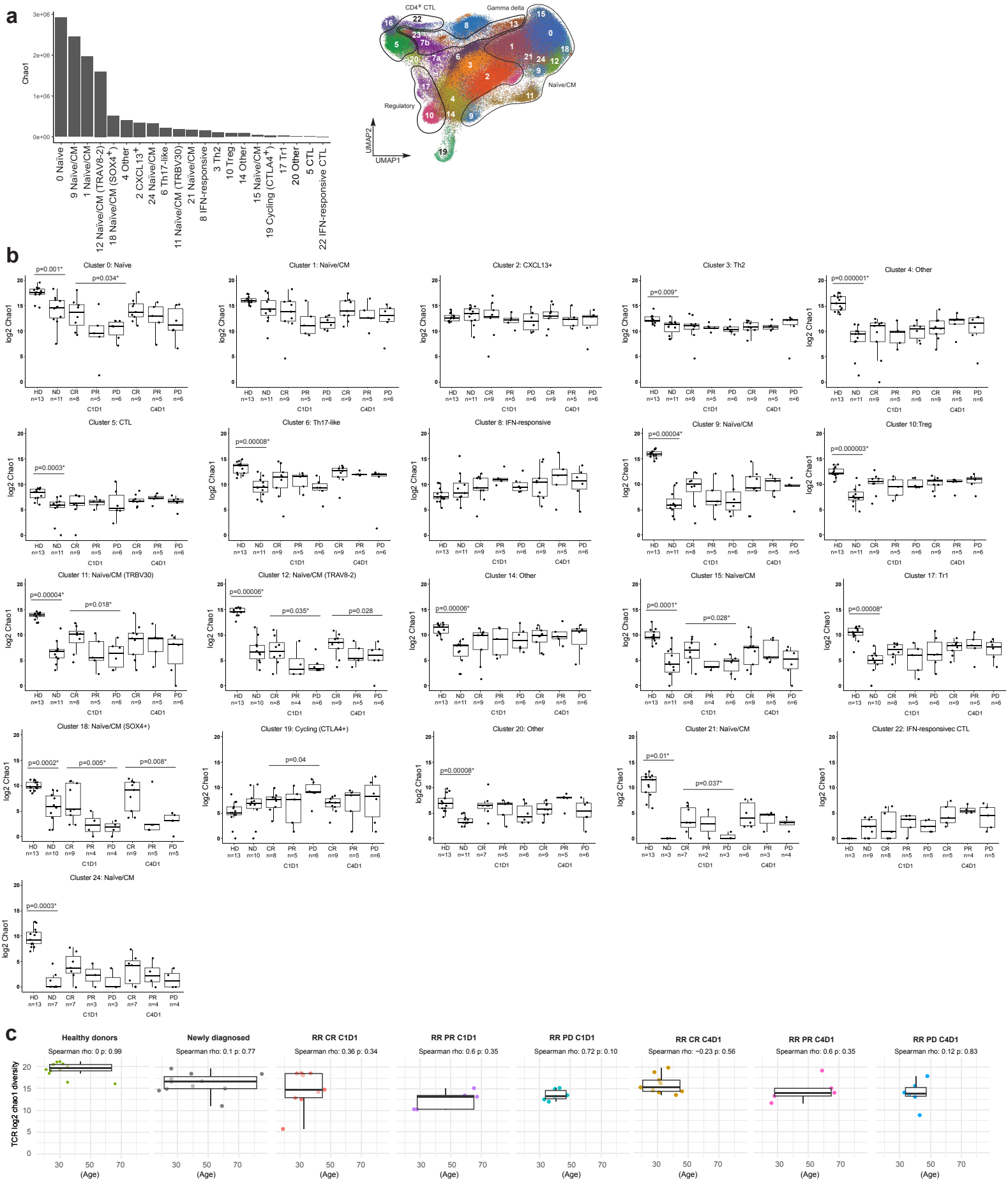

Supplementary Figure 4. TCR repertoire diversity of the CD3$^+$CD8$^-$ (CD4$^+$-enriched) immune cell clusters. a TCR repertoire diversity, as determined by Chao1 diversity index, across the CD3$^+$CD8$^-$ T-cell clusters. UMAP on the right for reference. **b** TCR repertoire diversity, as determined by log2 Chao1 diversity index, in CD3$^+$CD8$^-$ T-cell clusters from healthy donors (HD), patients with newly diagnosed (ND) cHL and patients with relapsed/refractory (R/R) cHL at baseline [C1D1] and C4D1 stratified by the best overall response (BOR) to PD-1 blockade. CR=Complete response, PR=partial response, PD=progressive disease. Differences between HD and patients with ND cHL were assessed by a two-sided Wilcoxon rank-sum test. A one-sided Cuzick trend test was used to compare patients with R/R cHL by BOR (CRs, PRs, and PDs). The indicated nominal p values were adjusted for multiple comparisons using the Benjamini-Hochberg methods and p values that remained significant FDR <0.1 are noted (*). **c** Correlation between patients' age (x-axis) and TCR log2 chao1 diversity of naive/CM CD4 T cells (y-axis) (Spearman correlation). **b-c** All box plots generated in R display the 25th and 75th percentiles (lower and upper hinges), median values, and whiskers. The whiskers extend from the hinges to the largest/smallest values within 1.5 times the interquartile range (IQR) from the hinge. Data points beyond the end of the whiskers are plotted individually. Source data are provided as a Source Data file.

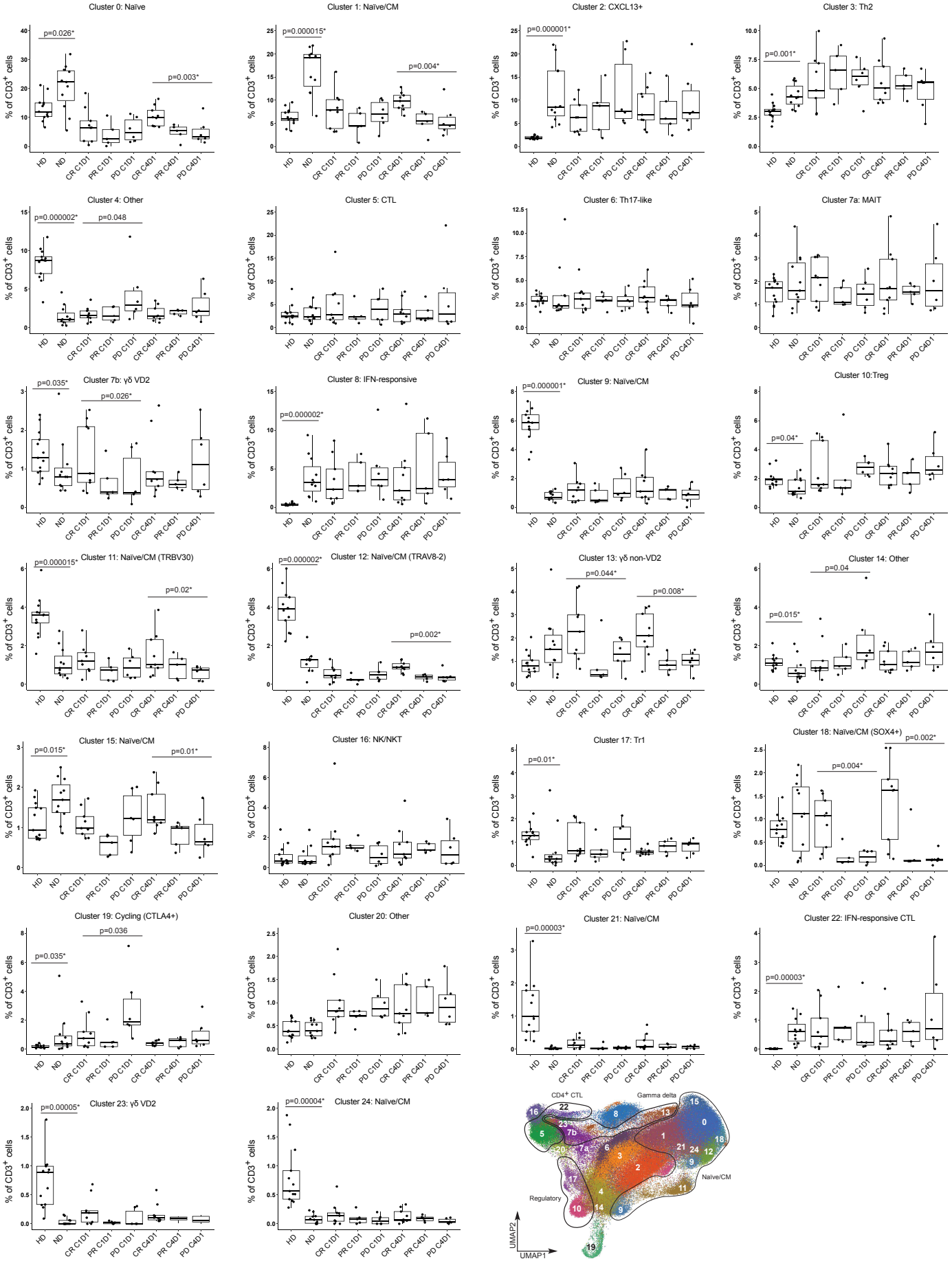

Supplementary Figure 5. Relative abundance of the circulating CD3⁺CD8⁻ (CD4⁺-enriched) clusters from healthy donors (HD, n=13) and patients with newly diagnosed (ND, n=11) cHL and patients with relapsed/refractory (R/R) cHL at baseline [C1D1] (n=20) and C4D1 (n=20) stratified by the best overall response (BOR) to PD-1 blockade. CR=Complete response (n=9), PR=partial response (n=5), PD=progressive disease (n=6). Differences between HD and patients with ND cHL were assessed by a two-sided Wilcoxon rank-sum test. A one-sided Cuzick trend test was used to compare patients with R/R cHL by BOR (CRs, PRs, and PDs). The indicated nominal p values were adjusted for multiple comparisons using the Benjamini-Hochberg methods; p values that remained significant after Benjamini–Hochberg correction FDR<0.1 are noted (*). UMAP at the bottom for reference. All box plots generated in R display the 25th and 75th percentiles (lower and upper hinges), median values, and whiskers. The whiskers extend from the hinges to the largest/smallest values within 1.5 times the interquartile range (IQR) from the hinge. Data points beyond the end of the whiskers are plotted individually. Source data are provided as a Source Data file.

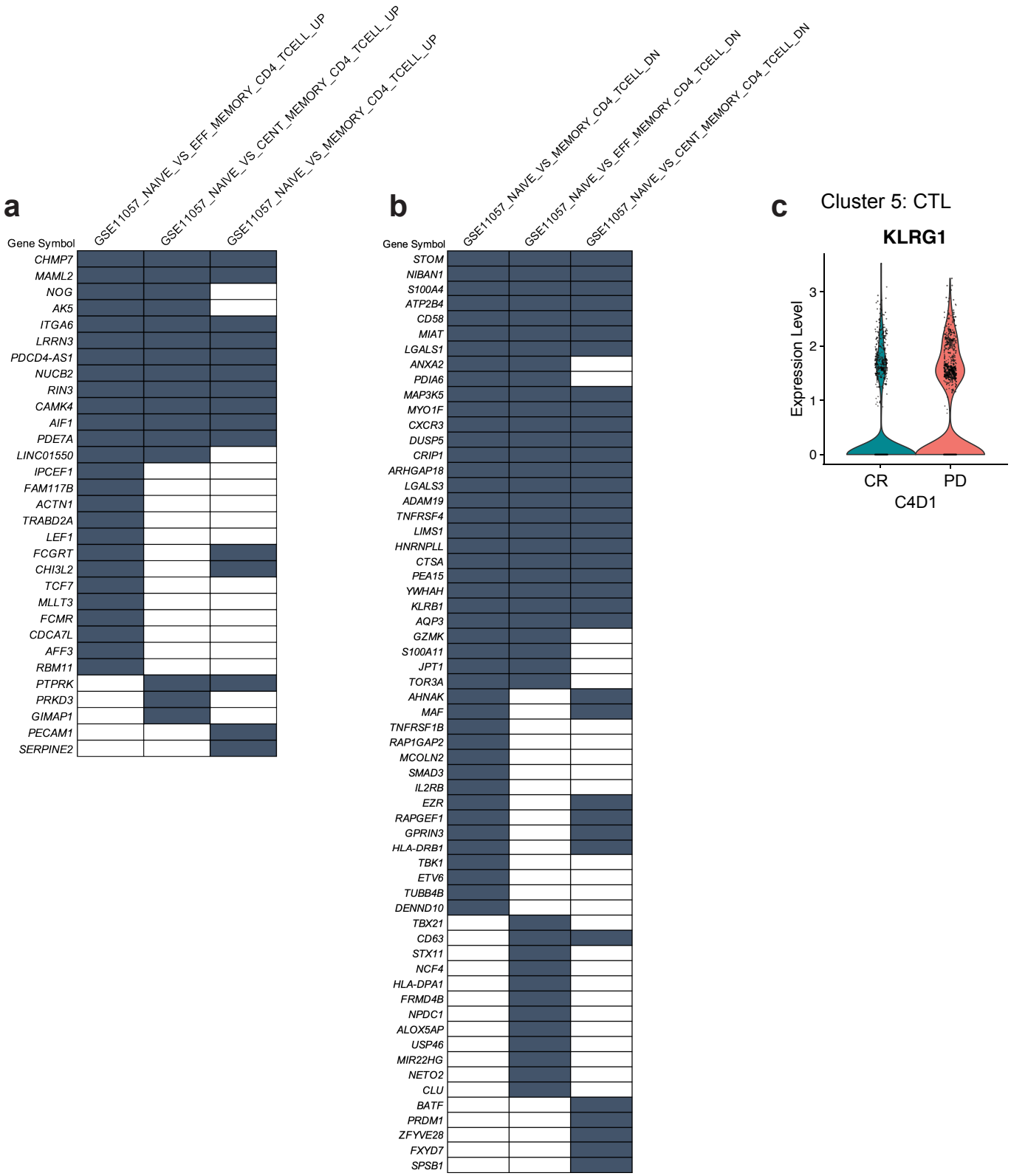

Supplementary Figure 6. Differential expression of response-related genes in CD4⁺ T cells. a-b Pathway enrichment analyses of response-related differentially expressed genes in the naïve/central memory (CM) CD4 T-cell clusters (0, 1, 9, 11, 12, 15, 18, 21 and 24) using Molecular Signatures Database (MSigDB) and C7: Immunologic gene sets. Results are based on a differential analysis of naive/CM CD4 T-cell transcripts in patients who achieved a CR or progressed (PD) on PD-1 blockade at C4D1. A two-sided permutation test, adjusted for multiple comparisons (adj p <0.1, fold change >1.5) was used to filter the differentially expressed genes in patients who achieved a CR or PD. **a** Transcripts that are more abundant in CRs than in PDs. **b** Transcripts that are less abundant in CRs than in PDs. **c** Violin plots showing the relative expression of *KLRG1* in Cluster 5: CTL in CRs versus PDs. The plot generated in R illustrates the data distribution with kernel density estimation. Plot displays the 25th and 75th percentiles (lower and upper hinges) and median values. The width of the violin at different points reflects the density of the data. Source data are provided as a Source Data file.

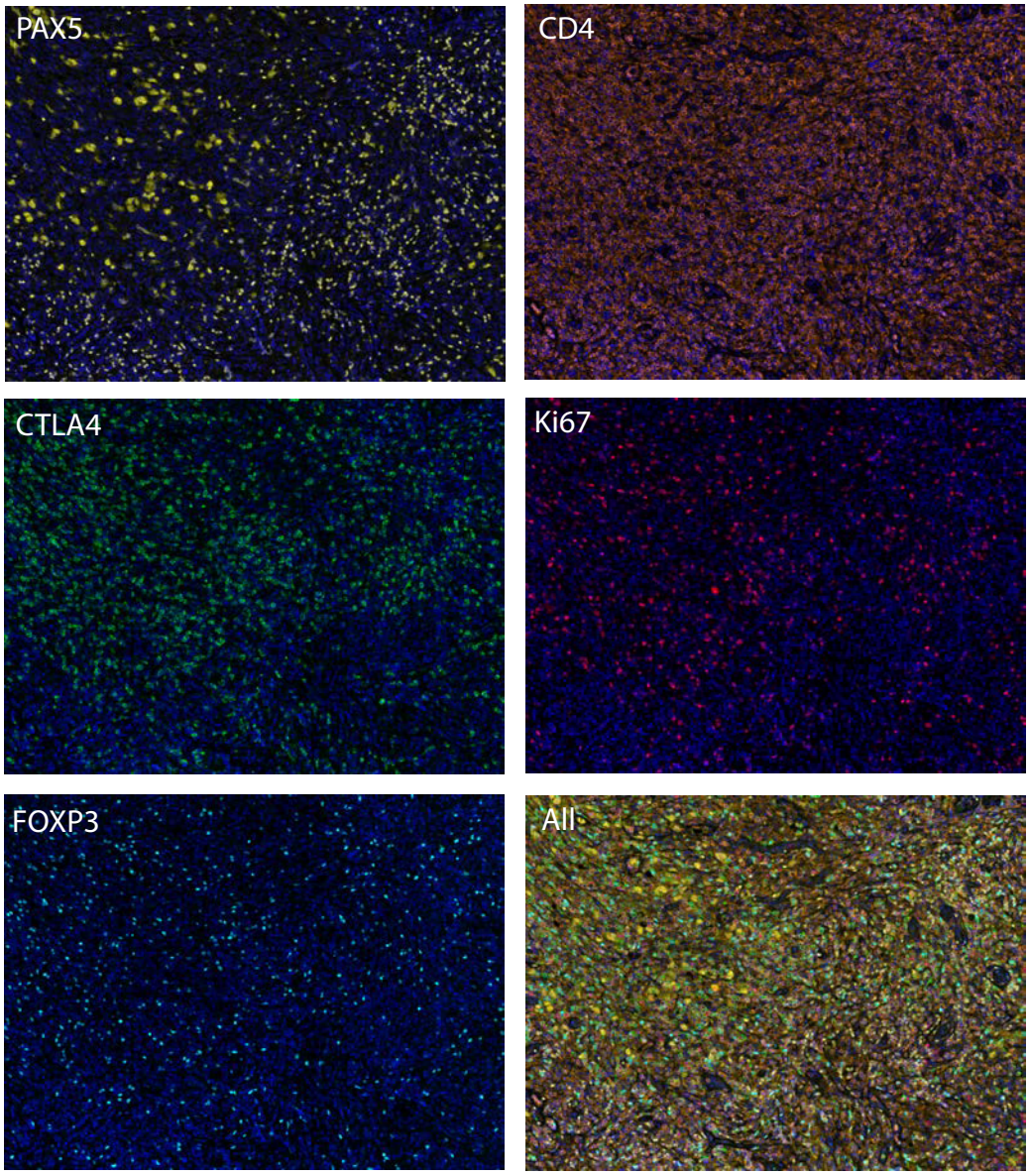

Supplementary Figure 7. Multiplex immunofluorescence imaging of CD4^{+}CTLA4^{+} cycling cells in the intact cHL tumor immune microenvironment. Single marker images of PAX5, CD4, CTLA4, Ki67 and FOXP3 staining by multiplex immunofluorescence of a representative newly diagnosed (ND) cHL. This experiment was performed in 9 ND cHL samples.

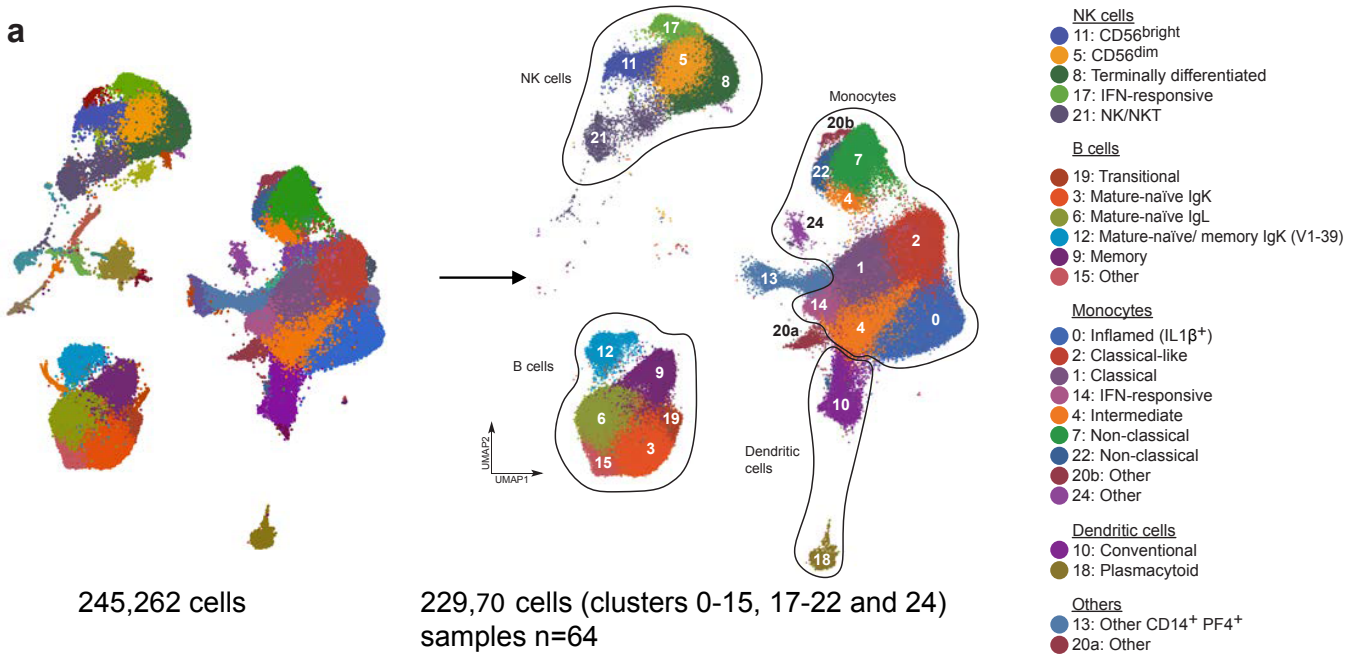

b CD3-, split by groups (cluster 0-24)

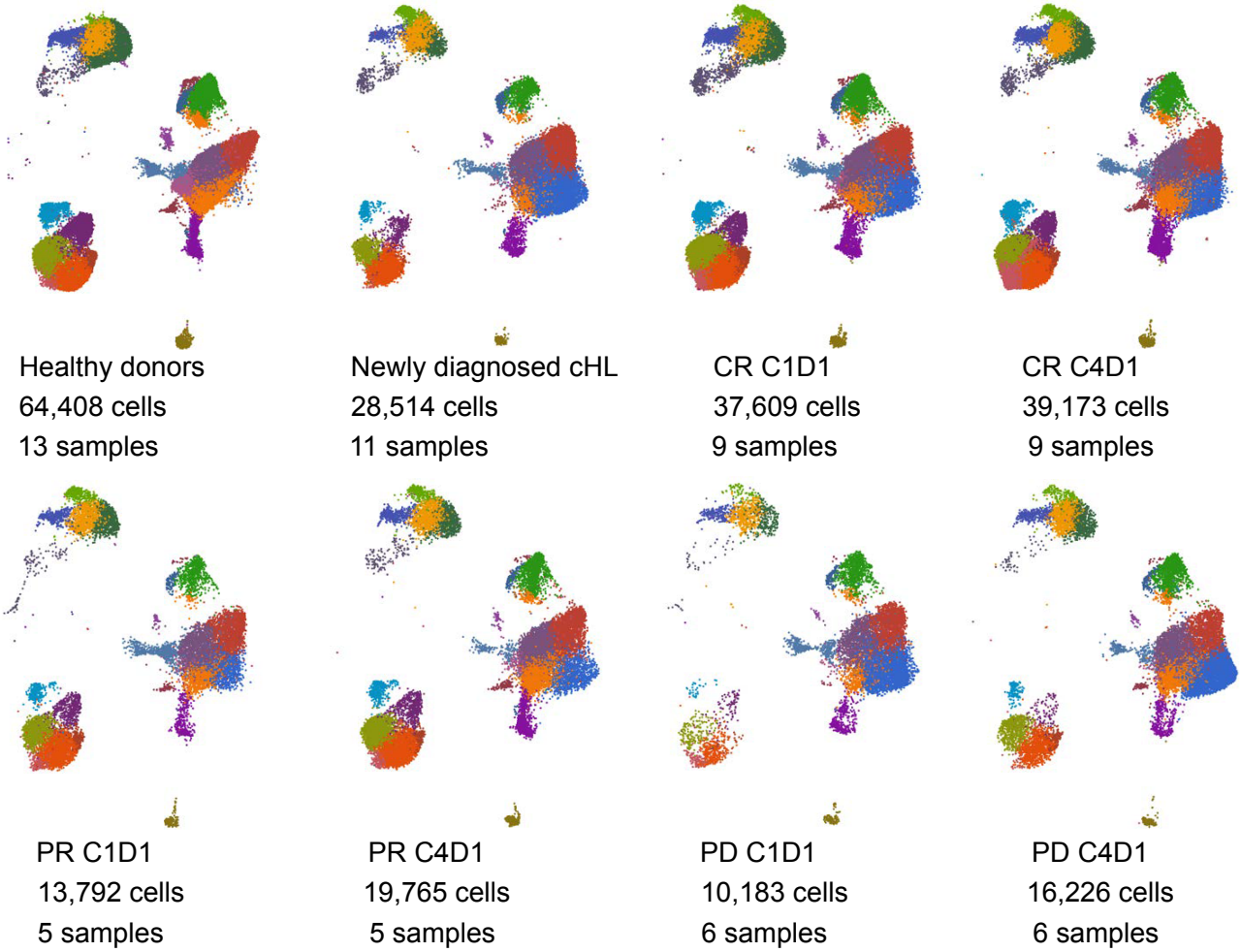

Supplementary Figure 8. Identification of circulating CD3- immune cell populations. a Uniform Manifold Approximation and Projection (UMAP) of CD3- single-cell expression profiles (n=245,262 individual cells) (left); Exclusion of clusters that did not meet the inclusion criteria and annotation of the remaining clusters (n=229,669 cells, clusters 0-15, 17-22 and 24) (right). **b** UMAP of CD3- single-cell expression profiles split by groups with the indicated number of cells and samples: HD, patients with ND cHL, R/R CR at C1D1, R/R CR at C4D1, R/R PR at C1D1, R/R PR at C4D1, R/R PD at C1D1, R/R PD at C4D1.

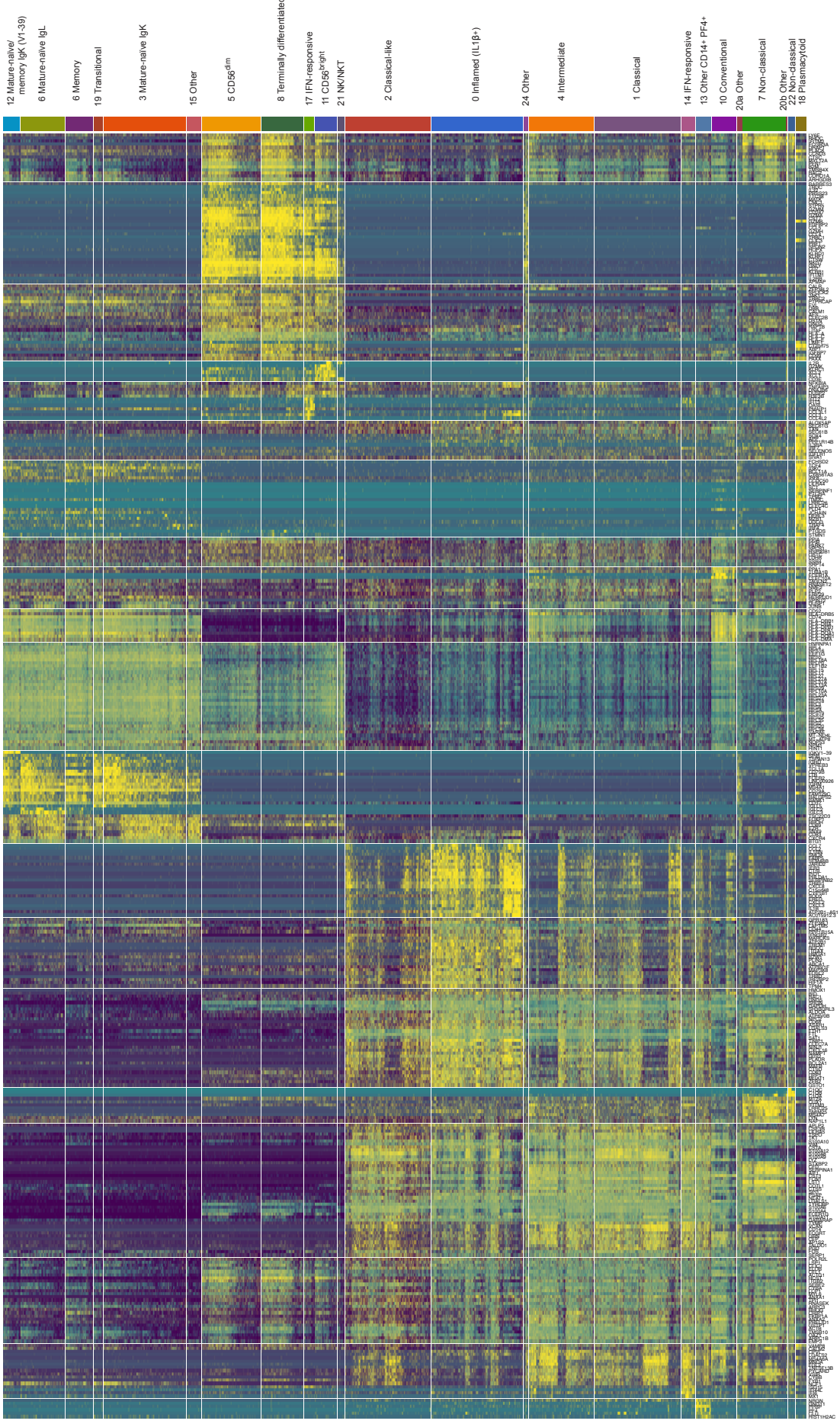

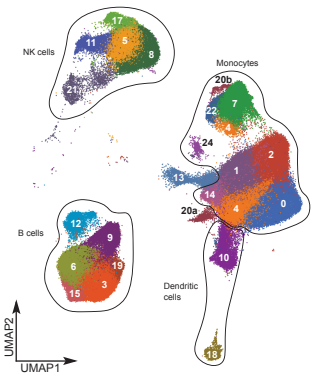

Supplementary Figure 9. Differential expression of marker genes in identified circulating CD3$^-$ immune cell clusters. Heatmap showing the relative expression (z-score normalized per gene) of the top differentially expressed genes that defined clusters in CD3$^+$CD8$^-$ space (a two-sided Wilcoxon rank sum test, adjusted for multiple comparisons, adj p <0.05, fold change >1.75).

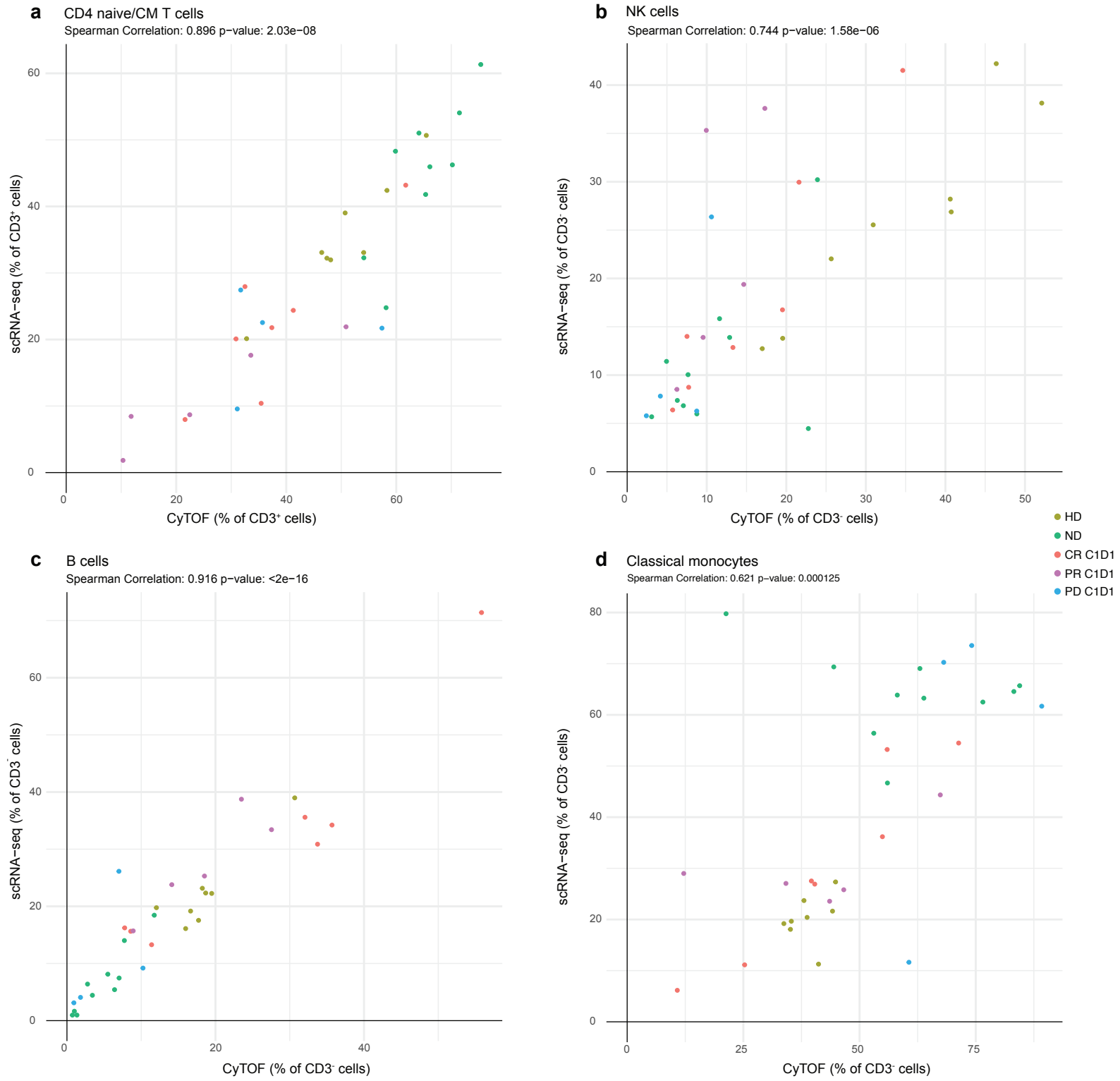

Supplementary Figure 10. Correlation between the abundance of (a) CD4 naive/CM T cells, (b) NK cells, (c) B cells, and (d) classical monocytes in serial peripheral blood aliquots from healthy donors (HD) and patients with cHL determined by CyTOF (reported in Cader et al Nat. Med. 26:1468-1479 [2020]) and scRNA-seq (this study). Protein-based CyTOF data and scRNA-seq analyses on serial aliquots of the same C1D1 peripheral blood mononuclear cell samples from 8 of 13 HD, 10 of 11 patients with newly diagnosed (ND) cHL, and 7 of 9 complete responders (CR), 5 of 5 partial responders (PR) and 4 of 6 patients with progressive disease (PD) are compared. Correlations between the abundance of these cell types as determined by flow cytometry (CyTOF) and scRNA seq were assessed using Spearman correlations. Source data are provided as a Source Data file.

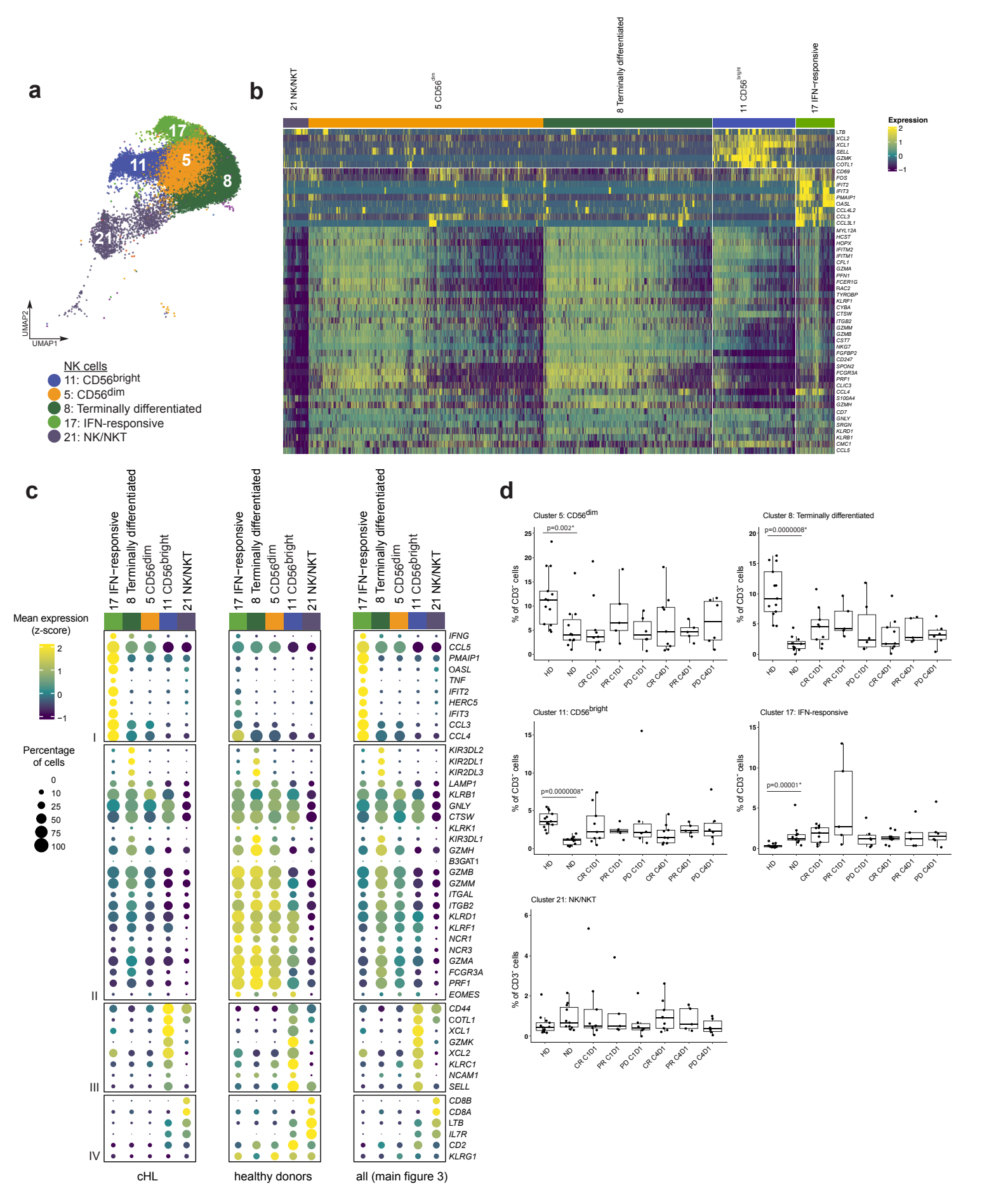

Supplementary Figure 11. Circulating NK-cell populations. a Annotated Uniform Manifold Approximation and Projection (UMAP) of NK-cell clusters (n=40,844 cells). **b** Heatmap showing the relative expression (z-score normalized per gene) of the top differentially expressed genes that defined NK-cell clusters (a two-sided Wilcoxon rank sum test, adjusted for multiple comparisons, adj p <0.05, fold change >1.75). **c** Dot plot with relative expression of selected genes in NK-cell clusters split by groups: all patients with cHL (left, n=51 samples), healthy donors (middle, n= 13 samples) and patients with cHL and healthy donors together (right, n=64 samples). Displayed genes were curated from the top differentially expressed genes that defined clusters using a two-sided Wilcoxon rank sum test, adjusted for multiple comparisons (adj p <0.05, fold change >1.75) and supplemented with relevant markers based on *a priori* knowledge. The size of the dot indicates the percentage of marker-expressing cells in each cluster and the z-score reflects mean marker expression across the clusters. **d** Relative abundance of NK-cell clusters in HD (n=13), patients with newly diagnosed (ND) cHL (n=11) and patients with relapsed/refractory R/R cHL at baseline [C1D1] (n=20) and on treatment [C4D1] (n=20) stratified by BOR to PD-1 blockade. Differences between HD and patients with ND cHL were assessed by a two-sided Wilcoxon rank-sum test. A one-sided Cuzick trend test was used to compare patients with R/R cHL by BOR (CRs, PRs, and PDs). The indicated nominal p values were adjusted for multiple comparisons using the Benjamini-Hochberg methods; p values that remained significant after Benjamini–Hochberg correction FDR<0.1 are noted (*). All box plots generated in R display the 25th and 75th percentiles (lower and upper hinges), median values, and whiskers. The whiskers extend from the hinges to the largest/smallest values within 1.5 times the interquartile range (IQR) from the hinge. Data points beyond the end of the whiskers are plotted individually. Source data are provided as a Source Data file.

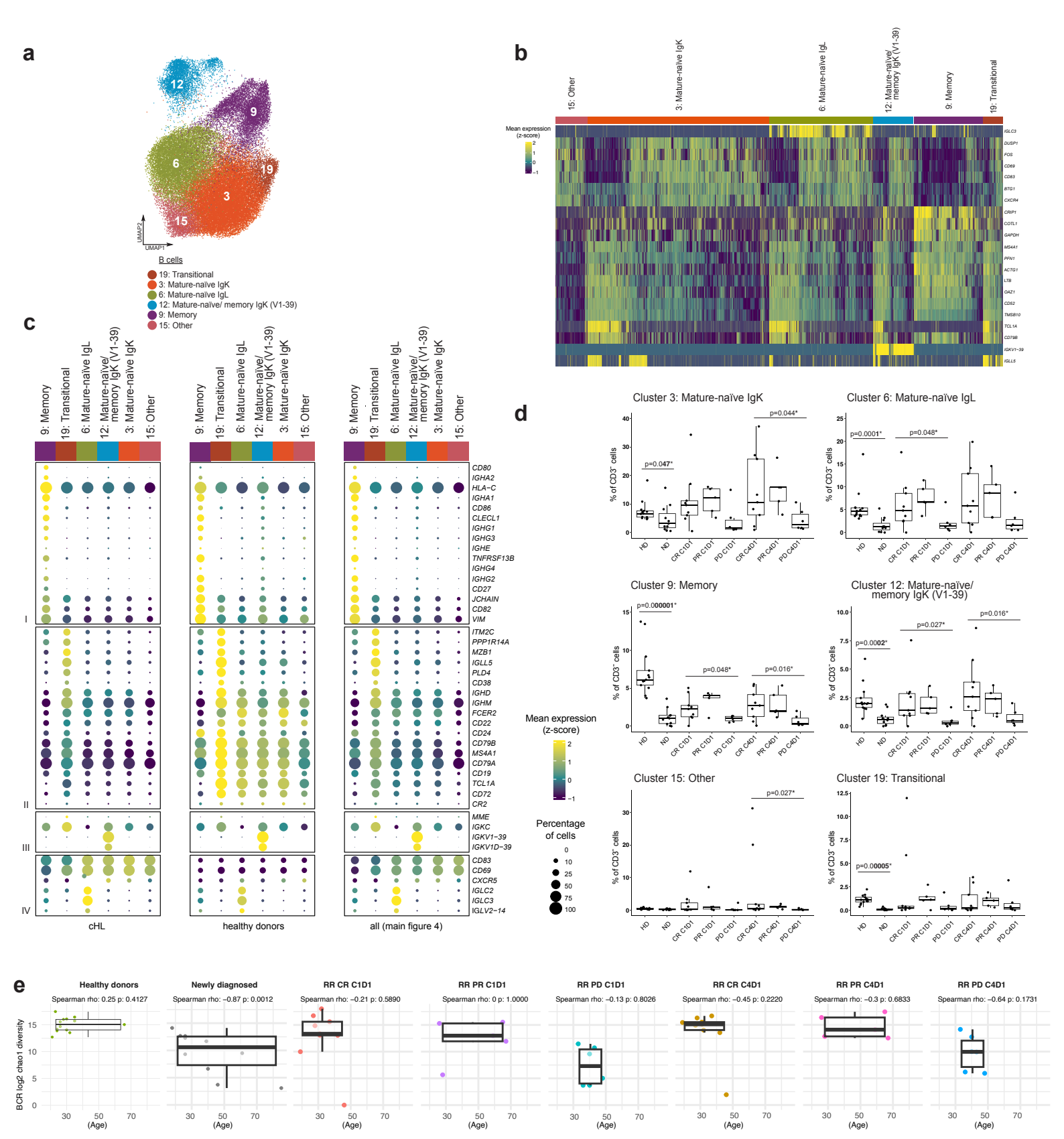

Supplementary Figure 12. Circulating B-cell populations. a Annotated Uniform Manifold Approximation and Projection (UMAP) of B-cell clusters (n=55,598 cells). **b** Heatmap showing the relative expression (z-score normalized per gene) of the top differentially expressed genes that defined B-cell clusters (adj p <0.05, FC >1.75). **c** Dot plot with relative expression of selected genes in B-cell clusters split by groups: all patients with cHL (left, n=51 samples), healthy donors (middle, n= 13 samples) and patients with cHL and healthy donors together (right, n=64 samples). Displayed genes were curated from the top differentially expressed genes that defined clusters using a two-sided Wilcoxon rank sum test, adjusted for multiple comparisons (adj p <0.05, fold change >1.75) and supplemented with relevant markers based on *a priori* knowledge. The size of the dot indicates the percentage of marker-expressing cells in each cluster and the z-score reflects mean marker expression across the clusters. **d** Relative abundance of B-cell clusters in HD (n=13), patients with newly diagnosed (ND) cHL (n=11) and patients with relapsed/refractory R/R cHL at baseline [C1D1] (n=20) and on treatment [C4D1] (n=20) stratified by BOR to PD-1 blockade. Differences between HD and patients with ND cHL were assessed by a two-sided Wilcoxon rank-sum test. A one-sided Cuzick trend test was used to compare patients with R/R cHL by BOR (CRs, PRs, and PDs). The indicated nominal p values were adjusted for multiple comparisons using the Benjamini-Hochberg methods; p values that remained significant after Benjamini–Hochberg correction FDR<0.1 are noted (*). All box plots generated in R display the 25th and 75th percentiles (lower and upper hinges), median values, and whiskers. The whiskers extend from the hinges to the largest/smallest values within 1.5 times the interquartile range (IQR) from the hinge. Data points beyond the end of the whiskers are plotted individually. **e** Correlation between patients' age (x-axis) and BCR log2 chao1 diversity of all B cells (y-axis) (Spearman correlation). Source data are provided as a Source Data file.

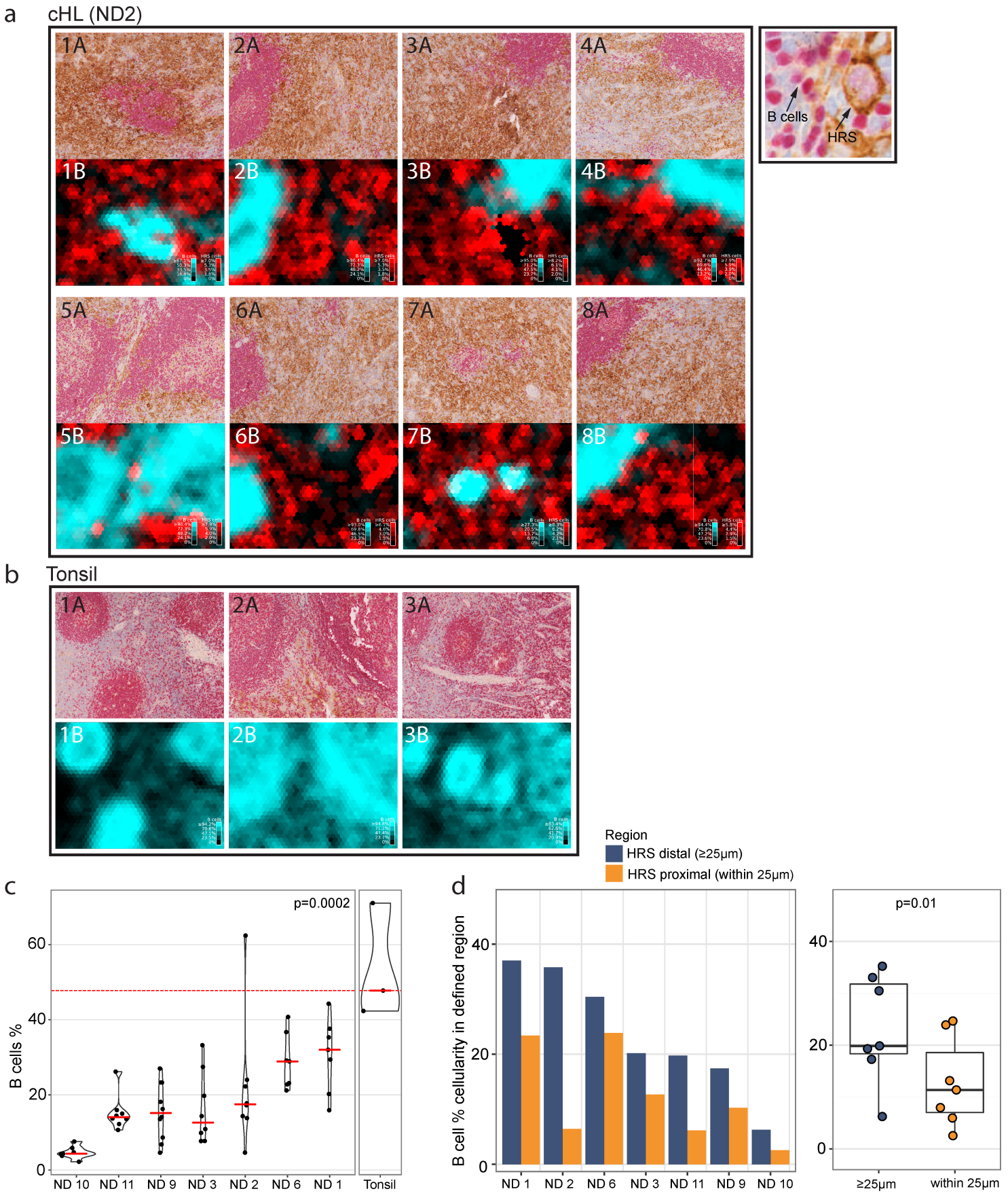

Supplementary Figure 13. Immunohistochemical analyses of normal infiltrating B cells in the intact cHL tumor immune microenvironment. a (Left, top panels, 1A-8A) Eight selected regions of interest (ROIs) of double PAX5 (red) and PD-L1 (brown) IHC images (17x magnification) from a representative newly diagnosed cHL (ND2). (Right upper panel). High magnification (57x) image of a larger PAX5^{dim} PD-L1^{+} HRS cell and additional smaller PAX5^{bright} normal B cells. (Left, bottom panels, 1B-8B) Composite heatmaps for PAX5^{dim} PD-L1^{+} HRS cells (red – high density of HRS cells) and PAX5^{bright} B cells (cyan – high density of B cells) overlaid on the original IHC images (from 1A-8A). The color intensities for each heatmap were determined by calculating the percentage of cells with the given phenotype (HRS: PAX5^{dim} PD-L1^{+}, B cells: PAX5^{bright}) among all cells within a 37µm radius distance of each hexagon's centroid. Each hexagon has a horizontal width (short diagonal) of 25 µm. The color scale for each ROI is shown in the lower right corner. This experiment was performed in 7 ND cHL samples **b** (Top panels, 1A-3A) Selected ROIs of double PAX5 (red) and PD-L1 (brown) IHC images (17x magnification) from a control tonsil. (Bottom panels, 1B-3B) Heatmaps for normal B cells (cyan – high density of PAX5^{bright} B cells) overlaid on the original IHC images (from 1A-3A). **c** Fraction of PAX5^{bright} B cells in the intact microenvironment of 7 newly diagnosed cHLs and a control tonsil. Each dot is a separately evaluated ROI. P value (0.0002, two-sided T-test) reflects the difference between the median normal B-cell percentage in the control tonsil and the 7 evaluated newly diagnosed cHLs. **d** B-cell cellularity in defined regions represented as % of normal B cells among all cells proximal to HRS cells (within 25µm, orange) or distal to HRS cells (>25µm, blue), paired for each individual case (left panel) and summarized for all cases together (right panel) (two-sided T-test). Source data are provided as a Source Data file.

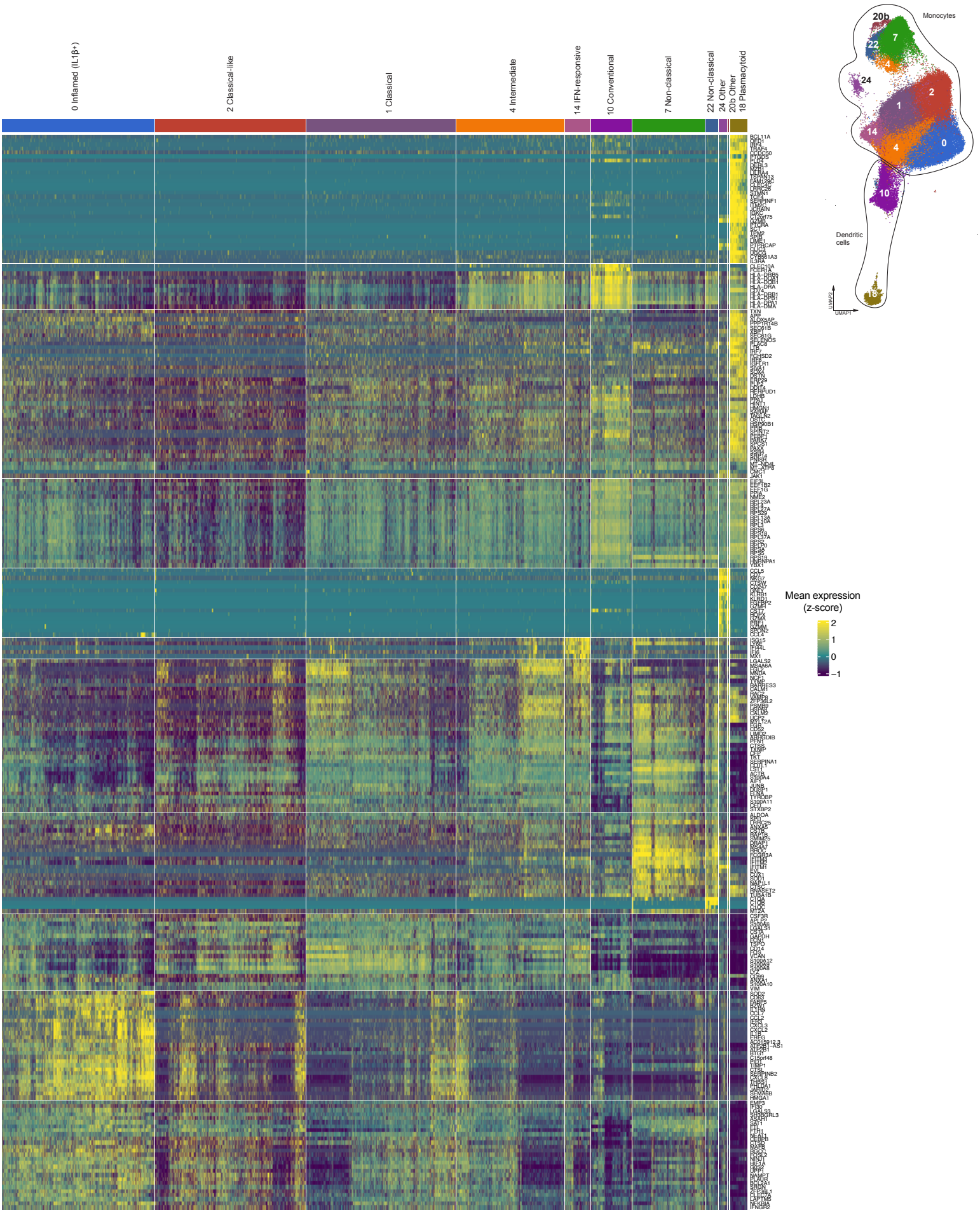

Supplementary Figure 14. Differential expression of marker genes in identified circulating myeloid clusters. Heatmap showing the relative expression (z-score normalized per gene) of the top differentially expressed genes that defined clusters in $CD3^-$ space (a two-sided Wilcoxon rank sum test, adjusted for multiple comparisons, adj p <0.05, fold change >1.75).

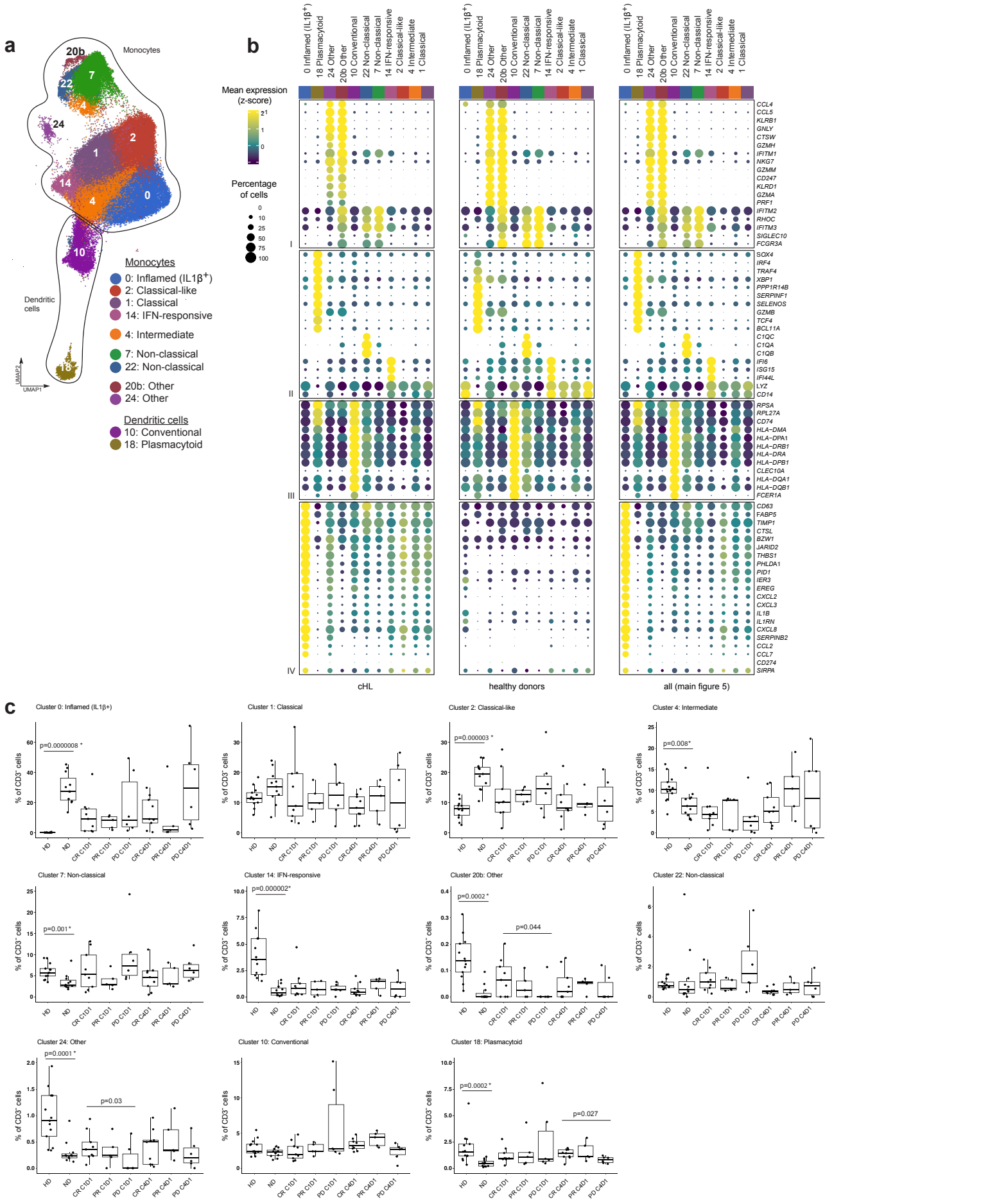

Supplementary Figure 15. Circulating myeloid populations. a Annotated Uniform Manifold Approximation and Projection (UMAP) of myeloid clusters (n=126,707 cells). **b** Dot plot with relative expression of selected genes in myeloid clusters split by groups: all patients with cHL (left, n=51 samples), healthy donors (middle, n= 13 samples) and patients with cHL and healthy donors together (right, n=64 samples). Displayed genes were curated from the top differentially expressed genes that defined clusters using a two-sided Wilcoxon rank sum test, adjusted for multiple comparisons (adj p <0.05, fold change >1.75) and supplemented with relevant markers based on *a priori* knowledge. The size of the dot indicates the percentage of marker-expressing cells in each cluster and the z-score reflects mean marker expression across the clusters. **c** Relative abundance of myeloid clusters in HD (n=13), patients with newly diagnosed (ND) cHL (n=11) and patients with relapsed/refractory R/R cHL at baseline [C1D1] (n=20) and on treatment [C4D1] (n=20) stratified by BOR to PD-1 blockade. Differences between HD and patients with ND cHL were assessed by a two-sided Wilcoxon rank-sum test. A one-sided Cuzick trend test was used to compare patients with R/R cHL by BOR (CRs, PRs, and PDs). The indicated nominal p values were adjusted for multiple comparisons using the Benjamini-Hochberg methods; p values that remained significant after Benjamini–Hochberg correction FDR<0.1 are noted (*). All box plots generated in R display the 25th and 75th percentiles (lower and upper hinges), median values, and whiskers. The whiskers extend from the hinges to the largest/smallest values within 1.5 times the interquartile range (IQR) from the hinge. Data points beyond the end of the whiskers are plotted individually. Source data are provided as a Source Data file.

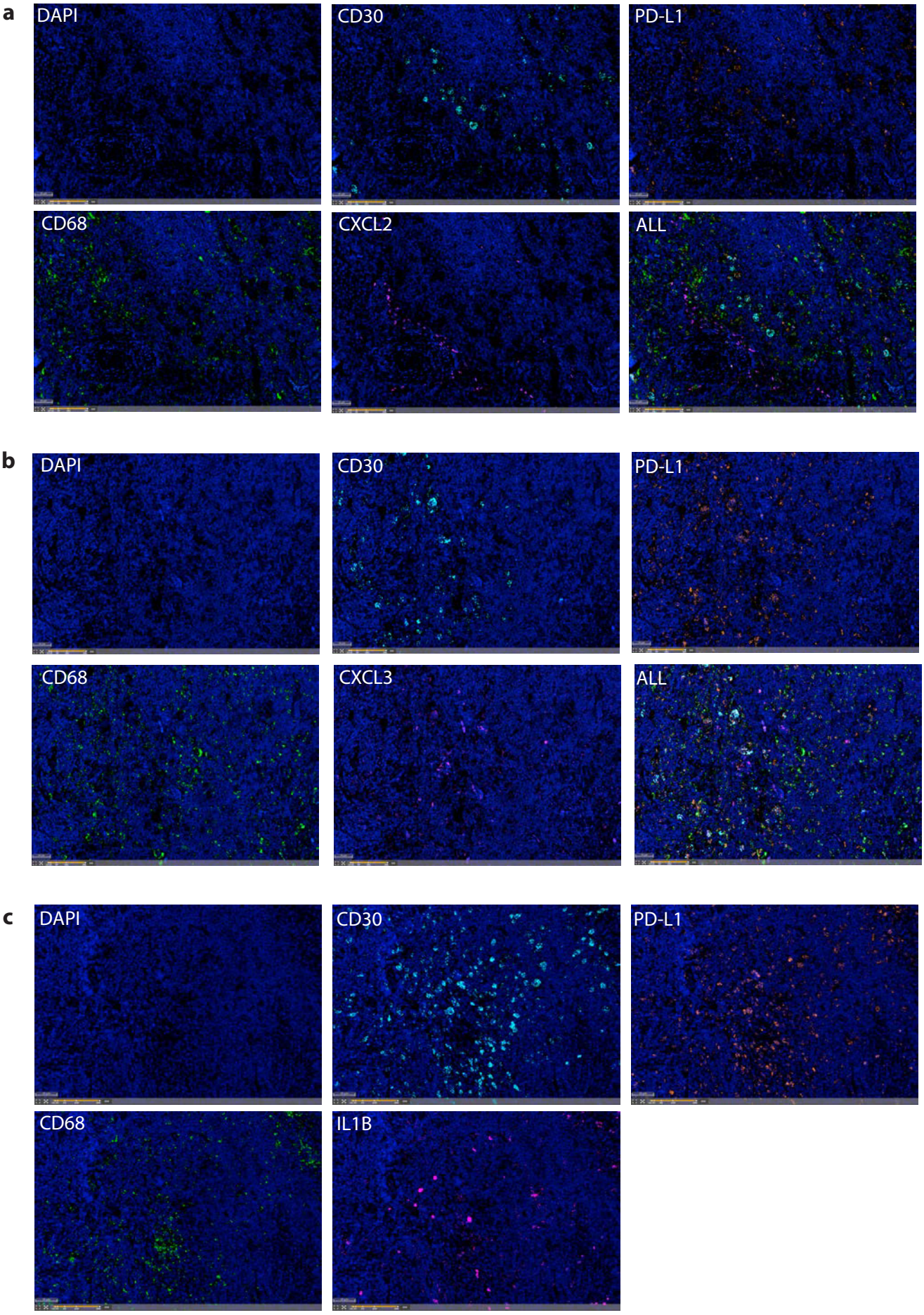

Supplementary Figure 16. RNAscope imaging of Cluster 0 monocyte/macrophages in the intact cHL tumor immune microenvironment. Single marker images of DAPI, *CD30*, *PD-L1*, *CD68*, *CXCL2* (**a**), *CXCL3* (**b**) and *IL1B* (**c**) staining by RNAscope multiplex immunofluorescence in a representative biopsy of newly diagnosed cHL. This experiment was performed in 4 ND cHL samples.

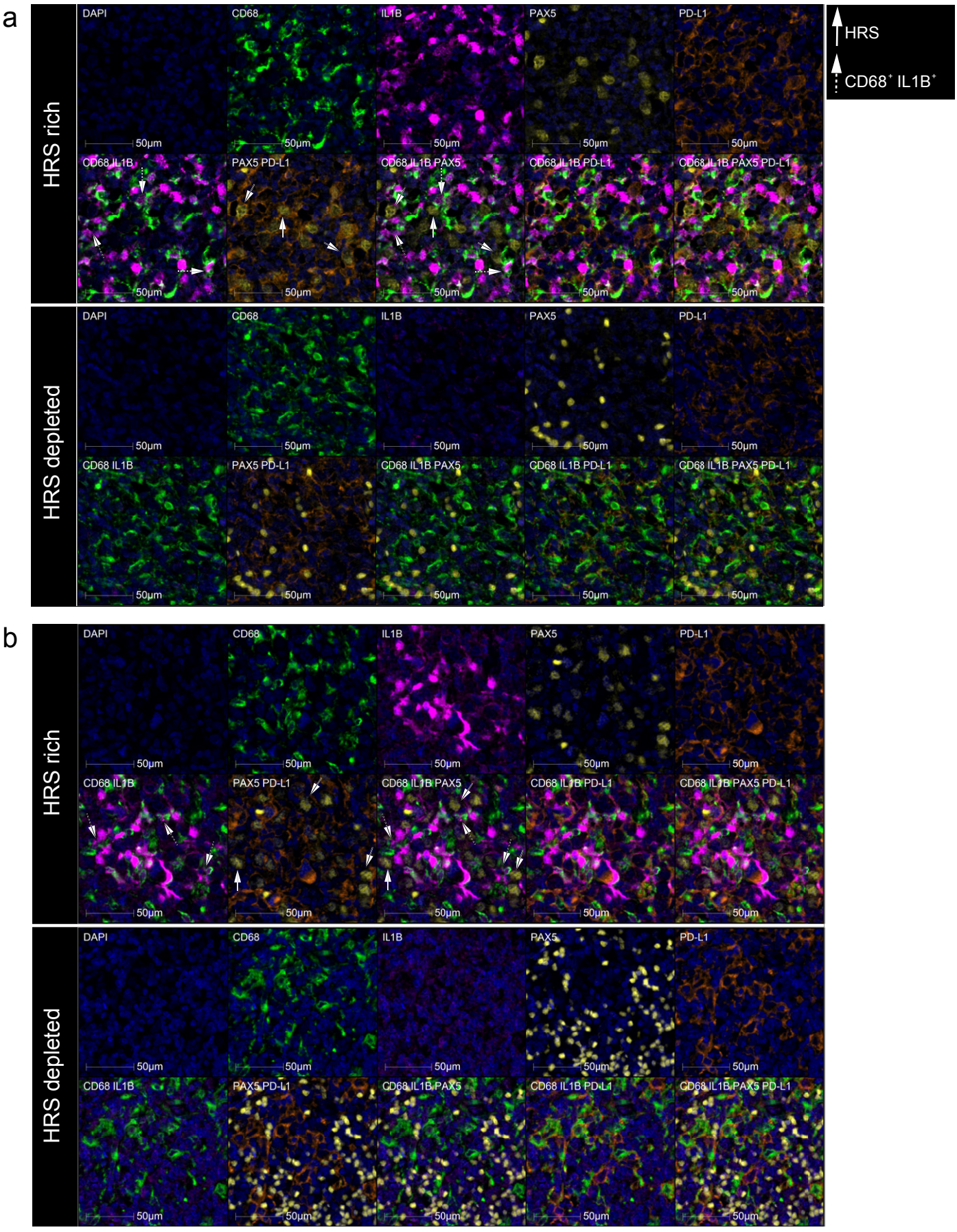

Supplementary Figure 17. Multiplex immunofluorescence imaging of IL1β^{+} monocyte/macrophages in the intact cHL tumor immune microenvironment. Two representative newly diagnosed cHLs (**a** and **b**) with regions including abundant PAX5^{dim} PD-L1^{+} HRS cells (upper panel) and rare HRS cells (lower panel) are shown. Arrows identify PAX5^{dim} PD-L1^{+} HRS cells and IL1β^{+} CD68^{+} monocytes/macrophages, which are co-localized in HRS-rich regions (upper panel). Regions with rare PAX5^{dim} PD-L1^{+} HRS cells primarily include smaller PAX5^{bright} normal B cells and IL1β^{-} CD68^{+} macrophages (bottom panel). *CD68* green, *IL1β* magenta, *PAX5* yellow and *PD-L1* orange. This experiment was performed in 4 ND cHL samples.

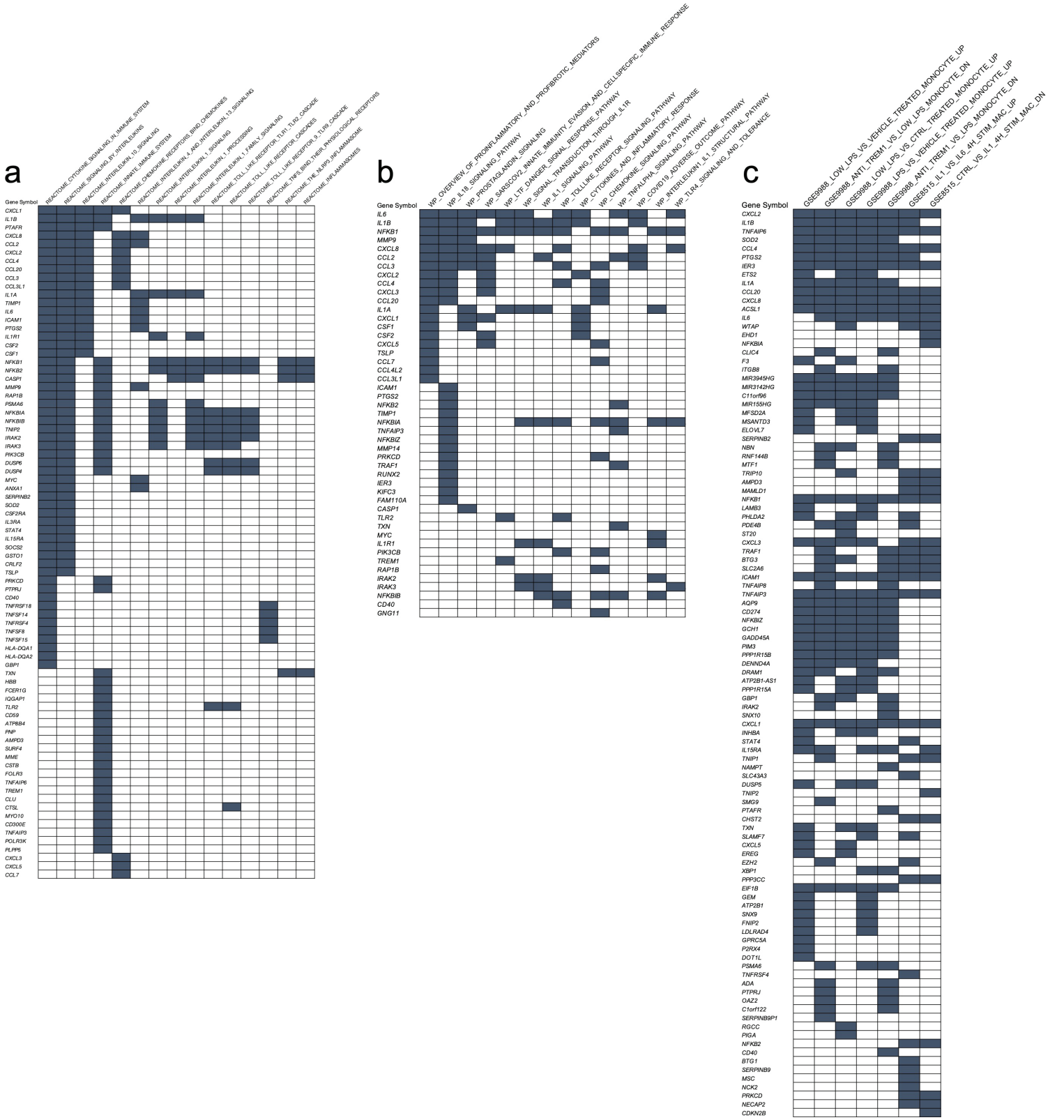

Supplementary Figure 18. Pathway enrichment analysis of response-related differentially expressed genes in circulating Cluster 0 monocytes using Molecular Signatures Database (MSigDB) and a CP:REACTOME: Reactome gene sets; **b** CP:WIKIPATHWAYS: WikiPathways gene sets; **c** C7: Immunologic gene sets.

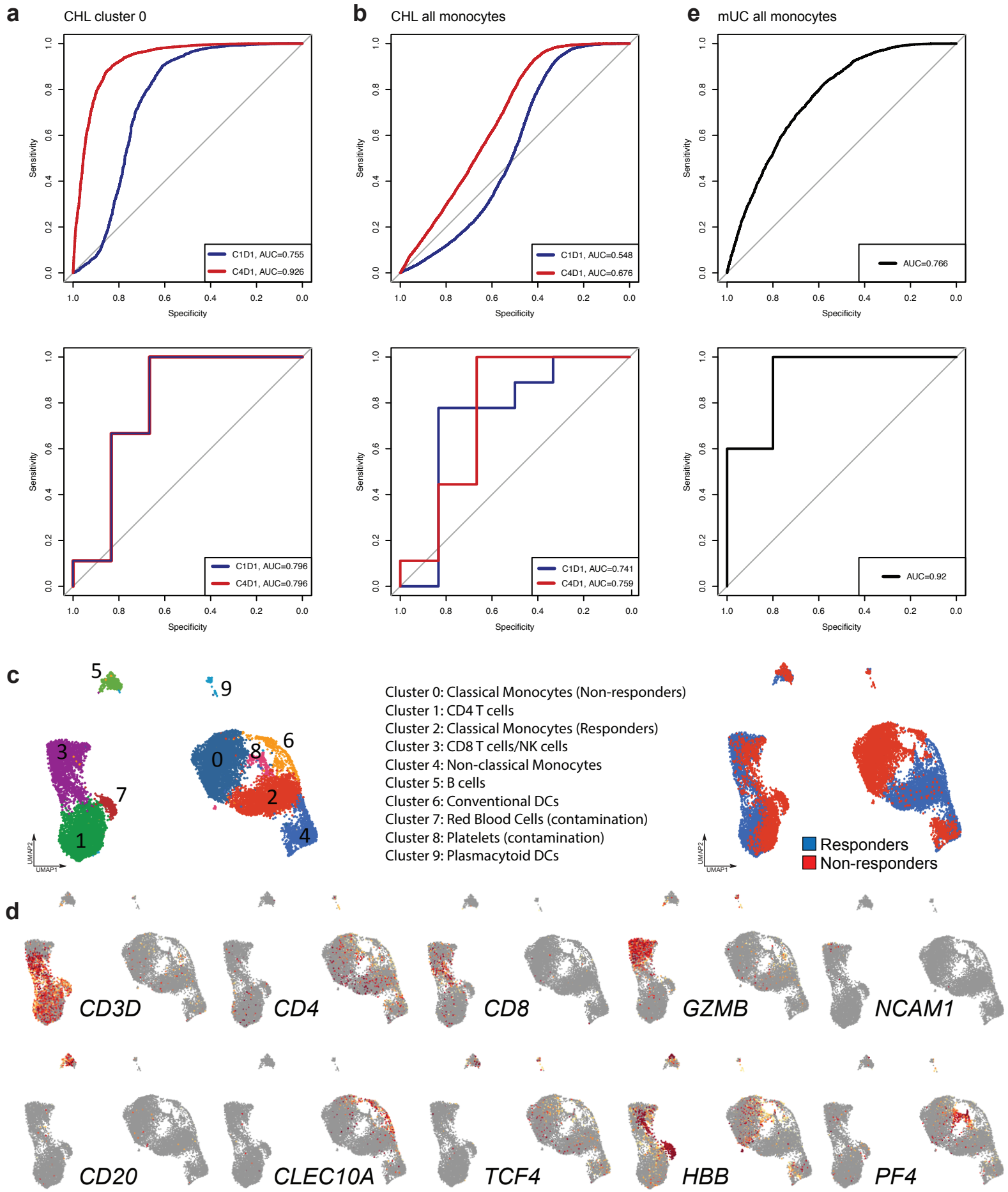

Supplementary Figure 19. ROC curves showing the sensitivity and specificity of the Cluster 0 AUCell transcriptional signature in cHL Cluster 0 monocytes at the single-cell (**a**, upper panel) and patient levels (**a**, lower panel), cHL all monocytes at the single-cell (**b**, upper panel) and patient levels (**b**, lower panel), and metastatic urothelial carcinoma all monocytes at the single-cell (**e**, upper panel) and patient levels (**e**, lower panel), (ref Figure 6c-e, main manuscript). **c-d** Annotation of immune cell clusters in an independent scRNA-seq dataset of metastatic urothelial carcinoma treated with PD-L1 blockade (n=10) (Yuen et al. Nat Med 26, 693-698 (2020)). **c** Annotated Uniform Manifold Approximation and Projection (UMAP) of single-cell expression profiles (n=14,474 cells) (left panel); annotated clusters filtered by the response to PD-L1 blockade (right panel). **d** Feature plots of selected cell lineage and differentiation markers.

CSF2	TM4SF1	AC024909.2	METTL7B	MAD1L1	PHLDA2	ZDHHC6	NKG7
IL6	TNFAIP8	CRLF2	SERPINB9	BNIP3	SNX10	IQGAP1	NAMPT
CXCL5	BATF3	PRDM8	NFKBIZ	SLC43A3	MMP9	TMEM38B	AD000671.2
TFPI2	SOD2	ACSL5	IL15RA	THBS1	IRAK2	RUNX2	PTAFR
TNFSF15	EREG	RNF144B	NFKBIA	CARD16	NFKB2	FNDC3B	MTSS1
F3	SERPINB2	SEMA3C	CLIC4	MIR4435-2HG	PIK3CB	PRMT2	IARS
ADAMTS6	MMP14	ITGB8	DOCK4	EHD1	MYO10	MMP24OS	GTPBP4
CXCL1	HILPDA	KMO	PPME1	FAM110A	SERTAD2	PTPRJ	ATXN1
CD274	TNFRSF18	NCR3LG1	TNIP1	CNDP2	RAPH1	SLC39A8	RGCC
MIR3142HG	CXCL8	TNFAIP3	KLF6	PIGA	MATK	DUSP4	ZSWIM4
CCL20	AC023157.3	AMPD3	POLR3K	PTRH1	TPMT	CETN2	KMT2E-AS1
LINC02426	MIR3945HG	KREMEN1	C15orf48	TNFRSF4	SPCS2	ANXA1	CAHM
PTGS2	STAT4	CTSL	MPZL1	TFB1M	XBP1	LONP1	KDM5B
AC026310.2	AF213884.3	N4BP3	GALNT6	NFKBIB	MRAS	AC016831.1	IL3RA
AC091808.1	CCL3L1	NCK2	ST20	PRKCD	DOT1L	AC123595.2	GSTO1
MIR155HG	CDKN2A	CSF1	TRIB3	MTF1	SLCO4A1	KLHL9	PNP
CCL3	MME	PPP3CC	ANXA5	RAB13	TNIP2	EIF1B	FLT1
TNFAIP6	TFPI	SOCS2	LINC01943	TNFSF8	CD300E	TMED5	TSLP
HMGA2	DUSP8	HLA-DQA2	AC007032.1	MGLL	OAZ2	DHRS9	
CXCL3	SERPINB9P1	AMZ1	MAP1LC3A	RAP1B	HBA1	ATP2B1	
CCL4	MFSD2A	ATP8B4	NOTCH2NL	TMEM106A	SEC61A1	LAMB3	
ZP3	NBN	FAM129A	AC002456.1	DENND4A	CDK14	HLA-DQA1	
IL1B	GNG11	AC017002.1	CLU	FCER1G	ANKRD28	CCDC18	
LINC00346	CCL7	ZDHHC9	EZH2	CHST2	MCTP1	MCRIP1	
TRAF1	AC004130.1	AC006449.6	C11orf96	SNX9	P2RX4	FAM20A	
IL1A	MIR210HG	EDNRB	SNX8	C1orf122	PLIN2	PPID	
NT5E	RRP1	CASP1	PDE4B	IER3	PIM3	LHFPL2	
MSC	SLC1A4	MS4A7	KCNN4	RUBCNL	IL1R1	DUSP5	
NRP1	SLC2A6	AC015912.3	UPB1	AC103591.3	HBB	GABPB1	
MSANTD3	IGFN1	TIMP1	METTL1	NBPF26	GPR137B	PPP1R15B	
LINC00926	AC025580.2	MEI1	TBC1D12	CD40	TMED9	MYDGF	
MSC-AS1	PGM3	SLFN5	ATP2B1-AS1	PHLDA1	BTG1	EMP1	
ELOVL7	PBX4	SDC2	NBPF9	VPS37C	FAM157C	IRAK3	
TRIP10	LINC00884	CREB5	TM4SF19	TDP2	TMEM208	AC004540.1	
DPYSL3	TTC28	LRP12	ARID5B	TSPAN3	KIFC3	TBC1D8	
CXCL2	SMG9	CSTB	SLC9A9	RABGEF1	TREM1	TNFSF14	
C16orf45	RHOBTB3	HEY1	DUSP6	PPP1R15A	KYNU	PPARD	
AC003092.1	BCAT1	NBPF19	BTG3	ADA	TRMT6	NPC1	
MREG	LDLRAD4	ASPH	GEM	GPRC5A	PDK1	SLC16A3	
SOWAHC	LINC01588	NDST2	PLAUR	PLPP5	TLR2	PDE4DIP	
INHBA	CCL4L2	SLC11A2	ST20-MTHFS	ACSL1	WTAP	FNIP2	
CDKN2B	CD59	SLC2A1	ETS2	OXSR1	SURF4	TPST1	
NRP2	GGT5	THAP2	GBP1	INF2	SPRY2	ZNF267	
SLAMF7	DRAM1	Z93930.2	ASAP1	ICAM1	CCDC71L	PSMA6	
AK4	DTX2	GADD45A	TMEM158	CSF2RA	TRIO	FOLR3	
STC1	TOMM34	LRBA	GCH1	SMS	PID1	MYL6	
SEPT10	ANGPTL4	MYC	MMP19	AQP9	DMXL2	HK2	
LINC01215	ADORA2A	AC025164.1	ALG2	OSBPL8	UFM1	NECAP2	
CCL2	MAMLD1	CRADD	TXN	ST3GAL1	HIST3H2A	SBNO2	
SLC7A11	MAML2	NFKB1	MCTP2	CITED2	ATP13A3	ZNF655	

Supplementary Table 1. Differentially expressed genes in circulating Cluster 0 IL1B+ monocytes. Differential expression analysis of response-related Cluster 0 transcripts in patients with relapsed/refractory (R/R) cHL who achieved a complete response (CR) or progressed on PD-1 blockade (PD). A two-sided permutation test, adjusted for multiple comparisons (adj p <0.1, fold change >1.5) was used to filter the differentially expressed Cluster 0 genes in patients who achieved a CR or progressed on therapy at C4D1.

A

Gene Name	Accession No	Target Region [Base Pairs (bp)]	Company	Catalog #	Channel	Probe Dilution	Fluor	Fluor Dilution
CD68	NM_001040059.1	367 - 1149	ACD	560598	1	1:50	Opal 520	1:1000
CD274-C3	NM_014143.3	124 - 1122	ACD	600868-C3	3	1:50	Opal 620	1:1000
CD30-C4	NM_152942.2	835 - 2165	ACD	310838-C4	4	1:50	Opal 690	1:1000
IL1B-C2	NM_000576	2 - 1319	ACD	310368-C2	2	1:50	Opal 570	1:1000
CXCL2-C2	NM_002089.3	9 - 1164	ACD	425258-C2	2	1:50	Opal 570	1:1000
CXCL3-C2	NM_002090.3	362 - 1059	ACD	1002158-C2	2	1:50	Opal 570	1:1000

B

Antigen	Clone	Company	Catalog #	Antibody Dilution	Diluent	Antigen Retrieval, Time (min)
PAX 5	Clone 24/Pax-5 (RUO)	BD Biosciences	610862	1:100	Akoya	ER2, 30 mins
PD-L1	405.9A11	not applicable	G.J.F.19	1:100	Ab Discovery Diluent, Ventana Medical Systems	ER2, 30 mins

C

Antigen	Clone	Company	Catalog #	Secondary, Time (min)	Antibody Dilution	Diluent	Fluor	Fluor Dilution	Antigen Retrieval, Time (min)
PAX 5	Clone 24/Pax-5 (RUO)	BD Biosciences	610862	Post Primary (15 min), Polymer (10 min)	1:100	Akoya	Opal 570	1:100	ER2, 10 mins
CTLA-4	E2V1Z	Cell Signaling Technology	53560S	Polymer (10 min)	1:100	CST	Opal 520	1:100	ER2, 20 mins
CD4	4B12	Agilent Dako	M731001-2	Post Primary (15 min), Polymer (10 min)	1:200	DV	Opal 620	1:125	ER2, 20 mins
Ki67	MIB-1	Agilent Dako	GA62661-2	Opal Polymer HRP (10 min)	1:100	Akoya	Opal 690	1:175	ER1,20
FOXP3	D2W8E	Cell Signaling Technology	98377S	Polymer (10 min)	1:100	Akoya	Opal 480	1:200	ER2, 30 mins

Supplementary Table 2. List of probes that were used for RNAscope™ Multiplex Fluorescent Assay (a) and antibodies used for immunohistochemistry (b) and multiplex immunofluorescence (c).